



Modelling gaseous and particulate secondary compounds formation during atmospheric degradation of 2-amino-2-methyl-1-propanol (AMP)

Daphné Ladet^{1,2}, Yelva Roustan¹, Karine Sartelet¹, and Olivier Duclaux²

¹CEREA, ENPC, Institut Polytechnique de Paris, EDF R&D, Champs-sur-Marne, France

Correspondence: Daphné Ladet (daphne.ladet@enpc.fr), Yelva Roustan (yelva.roustan@enpc.fr), and Karine Sartelet (karine.sartelet@enpc.fr)

Abstract.

The use of amines in carbon capture may contribute to high atmospheric emission. Amines have been shown to contribute significantly to the formation of carcinogenic compounds and aerosols. AMP (2-amino-2-methyl-1-propanol (CH₃)₂(CH₂OH)CNH₂) is a benchmark amine in carbon capture solvents, but the mechanisms of its contribution to particle formation are not yet well understood. This study aims to investigate the formation of aminium nitrates in the gas and particle phases. In order to model both the mass and number concentrations of the particles formed, reaction pathways for the formation of extremely low volatile products are proposed, as well as nucleation parameterisation. The model is constrained using an atmospheric chamber experiment, where AMP oxidation products were measured, as well as nitric acid (NA) and AMP in the particulate phase. Considering different molecular clusters of the type NAnAMPm allowed us to introduce low-volatility organic compounds likely to partition into the particulate phase. We present a first method considering the formation of a dimer, NA2AMP2, with low volatility and subject to nucleation parameterization, allowing for accurate reproduction of the evolution of the total number and particle size distribution compared to the experiment. This representation highlights an overestimation of the nitrate mass, emphasizing that the AMP/NA ratio in the clusters may not be equivalent to 1/1. A second method aims to correct this overestimation of nitrate mass by introducing NA1AMP2 clusters, which significantly improve AMP/nitrate partitioning in the particulate phase.

1 Introduction

In a context of global warming, the reduction of atmospheric emissions of carbon dioxide (CO₂) is a decisive issue. Technologies of carbon capture (CC), utilization and storage, become an essential component to combat climate change by mitigating the CO₂ emissions from major industrial sources (Metz et al., 2005; Martin et al., 2012). The aim is to separate the carbon dioxide from other species and then store it. To achieve this, the most effective method is washing with an amine solvent (Martin et al.,

²Air Quality Laboratory, TotalEnergies R&D, Solaize, France





2012), such as the CESAR solvent consisting of a mixture of AMP (2-amino-2-methyl-1-propanol ((CH₃)₂(CH₂OH)CNH₂) and piperazine (Gouedard et al., 2012; Brúder et al., 2010; Manzolini et al., 2015; Benquet et al., 2021; Alam, 2024). Overall, the various studies agree on the efficiency of capture processes. A report by the IPCC in 2005 emphasized a capture capacity ranging from 80 to 95%, while the International Energy Agency (IEA) asserts an average capture capacity of around 90% (Metz et al., 2005; Bouckaert et al., 2021). For example, the CO₂ capture sites at Mongstad have a capture capacity ranging from 25,000 to 1,000,000 tonnes of CO₂ per year, which is comparable to the CCPilot 100+ at Ferrybridge, which captures approximately 36,000 tonnes of CO₂ per year (Gjernes et al., 2013; Manzoor et al., 2014). However, during the washing process, the amine can be degraded by oxidation or thermal decomposition, form fragments or react with other compounds present (Strazisar et al., 2003; Vevelstad et al., 2011; Rochelle, 2012; Thong et al., 2012). Small quantities of amine and degradation products may be released in the atmosphere with other gases after the washing process. Once in the atmosphere they are subject to atmospheric chemical degradation pathways. The most important pathways are oxidation by hydroxyl radical (OH) and formation of secondary aerosols (Manzoor et al., 2014; Nielsen et al., 2010, 2011; Chen et al., 2022; Ge et al., 2011; Murphy et al., 2007). Both can lead to the formation of compounds that are carcinogenic and harmful to the environment, like nitrosamine and nitramine. Additionally, these compounds are known to be quite hydrophilic, which implies that scavenged substances can be potentially responsible for water and environmental contamination. The atmospheric chemistry of nitrosamines also includes photolytic degradation, which plays a major role in reducing atmospheric concentration levels (Chen et al., 2018; Yu et al., 2017).

Based on Rao and Rubin (2002), Karl et al. (2014) estimates from 40,000 to 160,000 kg per year Monoethanolamine (MEA) emissions for a large-scale carbon capture site for a capture of 1 Mt of CO₂ per year. These orders of magnitude are also found in the estimates of Sharma and Azzi (2014) which estimated the MEA emission at 80,000 kg per year for capturing 1 Mt of CO₂. Amine emissions are also associated with direct emissions of particles and ammonia. In addition to the problems associated with the atmospheric oxidation of amines, ammonia, which is emitted in large quantities (Gouedard et al., 2012; Fredriksen and Jens, 2013; Koiwanit et al., 2014), is highly reactive in the atmosphere, particularly in the formation of secondary particles, and is known to be a major environmental pollutant, particularly for aquatic ecosystems (Heo et al., 2015; Backes et al., 2016; Erisman and Schaap, 2004).

In order to prepare the future deployment of amine based carbon capture process, impact studies need to be carried out, with the aim of anticipating future impacts on the environment and populations. Given the complex atmospheric chemistry of amines, as well as the direct emissions of particulates, ammonia and VOCs, chemistry-transport models (CTM) appear to be the most appropriate modeling tools. Indeed, CTMs can be used to set up a multiphase chemistry specific to amines, which would add to the current atmospheric chemistry schemes already implemented, as well as enabling long-range impact studies. In addition, weather variability provides a better understanding of nitrosamine degradation, with a better representation of photolysis, as well as dry and wet deposition processes. Many of the impact studies carried out on carbon capture processes focused only atmospheric gas-phase degradation reactions of amines (Karl et al., 2015, 2011; Manzoor et al., 2014; Knudsen et al., 2010). More recent studies discuss the implementation of particle formation in the chemical mechanisms of CTMs. Indeed, mechanisms such as SAPRC or CSIAMP-19 include the formation of aminium nitrates, resulting from a reaction





between amines and nitric acid (Carter, 2008; Li et al., 2020; Karl et al., 2012). These methods consider a gas phase scheme leading directly to the formation of aminium nitrates in the particulate phase following a simple kinetic law, without taking into account the partitioning between phases. Particle formation is the result of highly complex and varied atmospheric processes, and experiments in atmospheric chambers have highlighted this degradation pathway as one of the most important removal processes in the atmosphere, with 20-60% (Tan et al., 2021, 2020) of amine particles formed.

This work involves modelling the atmospheric chemistry of amines and representing the various degradation pathways so that they can be implemented in a CTM, in order to be able to assess potential environmental impacts and population exposure. We developed a chemical scheme for modeling the formation and ageing of aminium nitrates in the gas and particulate phases, and evaluated it by comparison with an experiment carried out in an atmospheric chamber (Tan et al., 2021). The SSH-aerosol box model (Sartelet et al., 2025) is used for chemistry and particle modelling, and the experiment focuses on the degradation of 2-amino-2-methyl-1-propanol ((CH₃)₂(CH₂OH)CNH₂, AMP).

The general objective of this work is to represent the distribution of AMP between the gaseous and particulate phases, in order to complement the modeling study carried out on gaseous compounds by Tan et al. (2021). The main difficulty is to represent the mass, number and particle size distribution of the species in a way that is consistent with the measurements.

70 2 Methods

85

2.1 Experimental context

The experiment on which this work is based comes from Tan et al. (2021). This experiment was carried out in the EUPHORE B atmospheric chamber in Valencia, Spain, and aims to gain a better understanding of the oxidative degradation of AMP with OH.

The concentrations of gaseous compounds were measured by aProton-Transfer-Reaction Time-of-Flight Mass Spectrometry (PTR-TOF-MS 8000) instrument. The particle size distribution was observed with a Scanning Mobility Particle Sizer (SMPS) with 13 nm to 750 nm as size range. Measures of concentrations in the particulate phase were derived from two other different analysers: a prototype Chemical Analysis of Aerosol Online (CHARON) interfaced to a PTR-TOF 8000 instrument with a 100-750 nm size range and an Aerosols Mass Spectrometer (C-ToF-AMS) instrument with a 50-600 nm size range, the measuring instruments also have an estimated uncertainty of 25% for uncalibrated compounds and 10% for calibrated compounds (AMP). (Tan et al. (2021); Eichler et al. (2015); Drewnick et al. (2005)).

The experiment was carried out on June 15, 2015. The chamber canopy was opened at 07:48:00 and about 10 minutes later, a flow of 0.3 µL/min of isopropyl nitrite (IPN) was injected to maintain high levels of hydroxyl radicals. The end of this experiment corresponds to the closing of the chamber canopy at 10:00:00.

A large number of nanometric particles was formed during the chamber preparation phase, when nitric acid (HNO₃) was injected as an impurity with NO (Tan et al., 2021). Analysis of the data measured by the SMPS, presented in panel right of Figure 1, shows particle size evolution as a function of time, implying a coarsening process such as condensation or coagulation. In addition, temporal analysis of the variation of total particle number, presented in panel left of Figure 1, confirms that





coagulation is taking place, explaining the decrease in total particle number at the end of the experiment. Moreover, at the start of the experiment, a sharp increase in the total number of particles is observed, suggesting a nucleation peak.

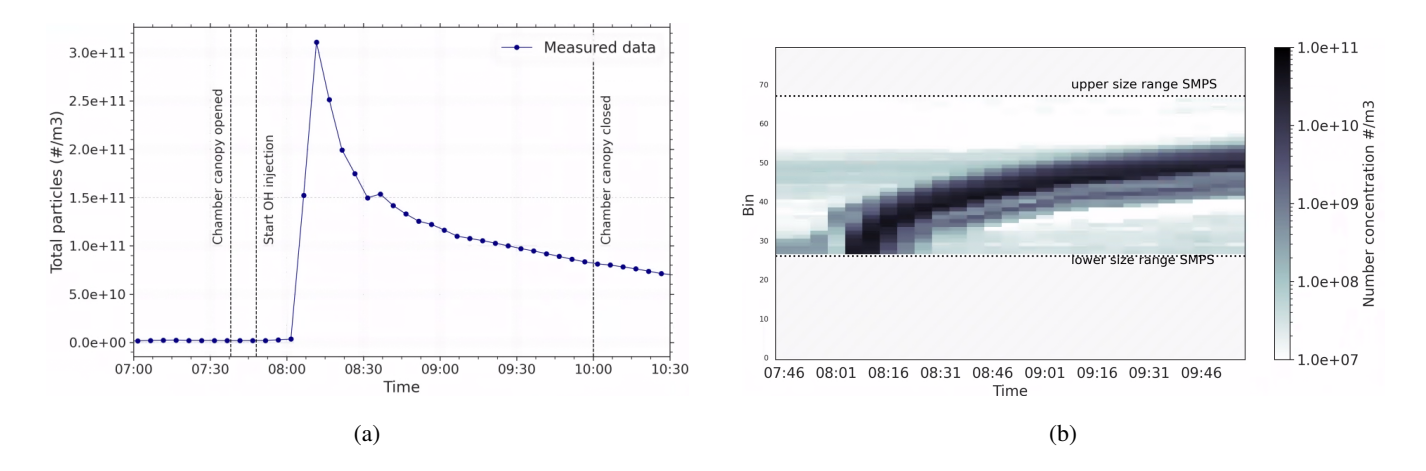


Figure 1. Temporal evolution of particle metrics: (a) total number of particles and (b) number concentration per size section.

2.2 Model methodology

100

105

The SSH-aerosol v2.0 box model [https://sshaerosol.wordpress.com/] (Sartelet et al., 2025, 2020) is used to represent physicochemical transformations of aerosols. This model is based on three modules: SCRAM (Size-Composition Resolved Aerosol Model) (Zhu et al., 2015) to represent the size distribution, SOAP (Secondary Organic Aerosol Processor) (Couvidat and Sartelet, 2015) for organic aerosol thermodynamic and H²O (Hydrophilic/Hydrophobic Organics mechanism) (Couvidat et al., 2012) for gas-phase chemistry. The thermodynamic of inorganic aerosols can be computed with ISORROPIA (Nenes et al., 1998) and several gaseous chemistry mechanisms are available. For example, the CB05 chemical mechanism (Yarwood et al., 2005), which describes the formation and evolution of oxidants, may be supplemented with additional gas-phase reactions that account for secondary organic aerosol (SOA) formation. SSH-aerosol has been widely used for comparison to chamber or flow-tube experiments (Sartelet et al., 2025; Lannuque et al., 2023; Sartelet et al., 2024; Wang et al., 2023; Lannuque and Sartelet, 2024). Figure 2 shows the processes considered in this work, integrating developments specific to the gaseous chemistry of amines, a representation of losses and chemistry specific to the EUPHORE atmospheric chamber, as well as the particle formation and evolution processes taken into account (coagulation, condensation/evaporation and nucleation). SSH-aerosol relies on a sectional approach to represent the size distribution of the aerosol particles population.

The atmospheric gaseous chemistry pathways of OH-initiated degradation of AMP have been implemented in CB05 based on Tan et al. (2021). Tan et al. (2021) carried out quantum calculations to compare theoretical kinetics with those measured, and adjusted some of the kinetic rates. The reaction scheme for AMP degradation initiated by oxidation with OH in the gas phase is presented in Table 1. The oxidation of AMP by OH forms different radicals, CH₃(CHO)CNH₂ (AMPal), (CH₃)(CH₂OH)C=NH (IPP) and (CH₃)₂(CH₂OH)CNH the amino radical (AMPN). IPP and AMPal are two species that were



115

120

125

130



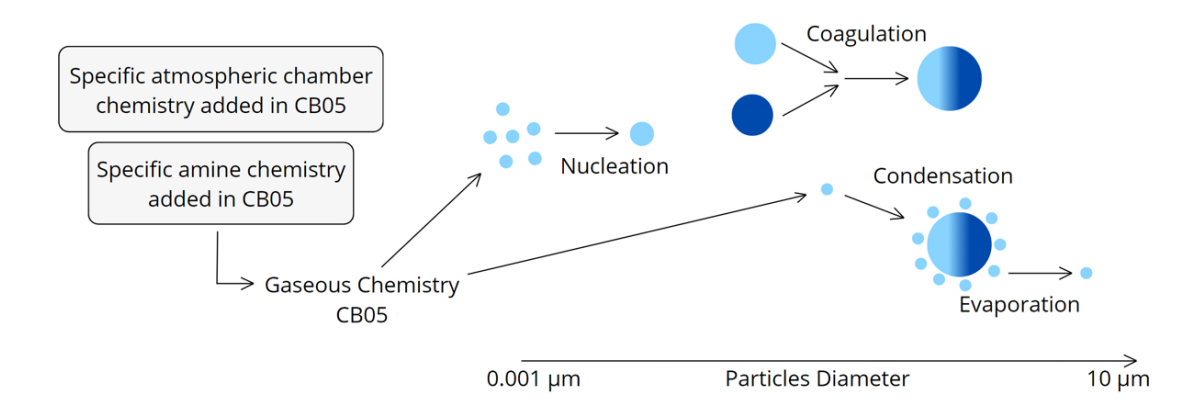
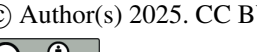


Figure 2. General scheme of atmospheric processes involves in aminium nitrate modelling with SSH-aerosol.

monitored with mass spectrometers, along with (CH₃)₂C=NH (P2IMI), an imine produced by oxidation of AMPal or dissociation of the amino radical. Nitramine (CH₃)₂(CH₂OH)CNHNO₂ (AMPNO₂) and nitrosamine (CH₃)₂(CH₂OH)CNHNO (AMPNO), are formed respectively following the reaction between NO₂ and NO with the amino radical. Some calculated kinetic constants have been adjusted based on the experiments, while respecting the uncertainty intervals given. The kinetic rate coefficient of reaction 1 has been set as 3.5×10^{-11} cm³.molecules⁻¹.s⁻¹, which is consistent with the calculated rate coefficient (at 298 K) and the experimental value (at 300 K), respectively: 3.6×10^{-11} cm³.molecules⁻¹.s⁻¹ and $(2.8 \pm 0.5) \times 10^{-11}$ cm³.molecules⁻¹.s⁻¹ (Tan et al., 2021). The second kinetic coefficient rate that has been adapted is related to the dissociation reaction 5. Indeed, the value presented in Tan et al. (2021) reaction mechanism applies a scaling factor of 0.2 on the theoretical results which lead to 4.6×10^{-3} s⁻¹. For the purposes of this study, the initial theoretical value of 2.3×10^{-2} s⁻¹ has been assumed. However, the branching ratios were conserved for the degradation products formed following oxidation of AMP with OH, i.e.: BCH3/BCH2/BNH2 = 6:70:24. The species monitored by PTR-MS-ToF, the main species (imine, nitrosamine, and nitramine), and the reactive compounds have been explicitly represented in the mechanism, because they will be tracked during this experiment. All other compounds, including acetamide (CH₃C(O)NH₂) formed during the oxidation of AMP and AM-Pal (R1 and R2), nitrogen compounds CH₃CN formed during the oxidation of P2IMI (R3), (CH₃)C(CHO)C=NH formed in the oxidation reaction of IPP (R4), (CH₃)₂(CHO)=CNHNO₂ formed by oxidation of nitramine (R10) have been decomposed according to the CB05 matrix of assignments (Yarwood et al., 2005).

In addition, representation of secondary aerosol formation from amine compounds represents a major degradation pathway in atmospheric conditions. Amines and aminium salts may partition between gaseous and particulate phases which makes this a complex system (Ge et al., 2011; Murphy et al., 2007; Chen et al., 2022; Shen et al., 2023; Qiu and Zhang, 2013; Kumar et al., 2018). Indeed, amines are known to have a predisposition to react with acids present in the atmosphere, due to their highly basic nature. The salts formed are often regarded as non-volatile due to a lack of information on equilibrium constants, although dissociation is possible (Carter, 2008; Murphy et al., 2007).



140



Table 1. AMP gaseous degradation pathways (Tan et al., 2021; Carter, 2008) in atmospheric conditions employed in the model, ^a bimolecular rate coefficients (in cm³.molecules⁻¹.s⁻¹) and ^b unimolecular rate coefficients (in s⁻¹). ALDX represents Propionaldehyde and higher aldehydes equivalent to 2 reactive carbons, PAR represents Paraffin carbon bond (C-C) equivalent to 1 reactive carbon, acetone was described as three PAR and other species follow example and bond distributions according to the CB05 matrix of assignments. These species are part of the CB05 mechanism included in SSH-aerosol and are used to represent VOCs.For amine species and degradation compounds we have : 2-amino-2-methyl-1-propanol ((CH₃)₂(CH₂OH)CNH₂, AMP); different radicals, CH₃(CHO)CNH₂ (AMPal), (CH₃)(CH₂OH)C=NH (IPP) and (CH₃)₂(CH₂OH)CNH the amino radical (AMPN); an imine (CH₃)₂C=NH (P2IMI); nitramine (CH₃)₂(CH₂OH)CNHNO₂ (AMPNO₂) and nitrosamine (CH₃)₂(CH₂OH)CNHNO (AMPNO).

N°	Reaction	Rate coefficient
	$(CH_3)_2(CH_2OH)CNH_2 + OH \longrightarrow 0.06 (CH_3)(CH_2OH)C=NH$	
1	+ 0.43 (CH ₃) ₂ (CHO)CNH ₂	$a 3.5 \times 10^{-11}$
1	+ 0.24 (CH ₃) ₂ (CH ₂ OH)CNH	5.5 × 10
	+ 0.27 ALDX	
2	$(CH_3)_2(CHO)CNH_2 + OH \longrightarrow 0.95 (CH_3)_2C=NH + 0.05 ALDX$	$a 7.0 \times 10^{-11}$
3	$(CH_3)_2C=NH+OH\longrightarrow CH_2O+PAR$	$a 2.0 \times 10^{-11}$
4	$(CH_3)(CH_2OH)C=NH+OH\longrightarrow ALDX+PAR$	$a 2.0 \times 10^{-11}$
5	$(\text{CH}_3)_2(\text{CH}_2\text{OH})\text{CNH} \longrightarrow (\text{CH}_3)_2\text{C=NH} + \text{CH}_2\text{O}$	$^{b}2.3 \times 10^{-2}$
6	$(\text{CH}_3)_2(\text{CH}_2\text{OH})\text{CNH} + \text{NO} \longrightarrow (\text{CH}_3)_2(\text{CH}_2\text{OH})\text{CNHNO}$	$^{a}(8.5\pm1.4)\times10^{-14}$
7	$(CH_3)_2(CH_2OH)CNH + NO_2 \longrightarrow (CH_3)_2(CH_2OH)CNHNO_2$	$^{a}(3.2\pm0.5)\times10^{-13}$
8	$(CH_3)_2(CH_2OH)CNHNO + OH \longrightarrow CH_2O + NO_2 + 3.0 PAR$	$a 1.0 \times 10^{-10}$
9	$(\text{CH}_3)_2(\text{CH}_2\text{OH})\text{CNHNO} + \text{h}\nu \longrightarrow (\text{CH}_3)_2(\text{CH}_2\text{OH})\text{CNH} + \text{NO}$	$^a0.34\times \mathrm{J}_{\mathrm{NO}_2}$
10	$(\text{CH}_3)_2(\text{CH}_2\text{OH})\text{CNHNO}_2 + \text{OH} \longrightarrow \text{ALDX} + 3.0 \text{ PAR}$	$^{a}1.4 \times 10^{-11}$

This work aims to develop a simple way of representing the formation of aminium salts from AMP, taking into account mass and number concentrations. In the context of AMP, and due to the high volatility of nitric acid, the aminium nitrate formed is semi-volatile with a saturation vapor pressure of about 9.75×10^{-8} torr (Tan et al., 2021), which is too high to allow nucleation (Chamba et al., 2023) and partitioning on ultrafine particles. Indeed, the nucleation of amines with nitric acid was first postulated by Karl et al. (2012) for monoethanolamine (MEA), presenting conclusive modeling on particle formation via this pathway.

Recent studies (Chee et al., 2019; Chen et al., 2024) present the results of quantum calculations on the stability of NAnR $_x$ NH $_y$ m clusters, where n represents the number of nitric acid (NA) molecules and m represents the number of amine (R $_x$ NH $_y$) molecules present in the clusters. Theses studies include evaporation and formation rates for clusters under specific conditions, as well as the influence of hydration, the main clustering pathways and clusters stability, including Gibbs free energy (Δ G), enthalpy (Δ H) and entropy (Δ S) values. The Gibbs free energy change of formation is defined as:



155

165



$$P8L\Delta G = \Delta H - T\Delta S \tag{1}$$

where ΔH is the enthalpy change, ΔS is the entropy change, and T is the temperature. The Gibbs free energies of bonding can then be used to recalculate the saturated vapor pressure above the surface of the clusters, as follows:

$$P_{\text{sat}} = P^o \times \exp(-\frac{\Delta G_{\text{vap}}}{RT}) \tag{2}$$

where R is the ideal gas constant, T is the temperature, P^o is the atmospheric pressure, $\Delta G_{\rm vap}$ is the Gibbs free energy change of vaporization. This equation is derived from a criteria of thermodynamic equilibrium between the liquid and vapor phases, obtained by expressing the variation in Gibbs free energy as a function of pressure according to:

150
$$\mu = \mu^o + RT \ln(P/P^o)$$
 (3)

where μ denotes the chemical potential (or molar Gibbs free energy) of a species at a given pressure, and μ^o corresponds to the standard chemical potential (i.e., the value of μ at P^o). $\Delta G_{\rm vap}$ physically represents the transition of one mole of liquid to vapor, implying that for low (or negative) values, evaporation will be more spontaneous than in cases with high (or positive) values. This equation therefore reflects a compound's tendency to evaporate, implying that the lower $P_{\rm sat}$ is, the more the compound will tend to remain in the condensed phase.

For the case of Dimethylamine (DMA), Gibbs bonding free energies are used here to estimate the saturation vapor pressures of clusters. The saturation vapor pressure of NA1DMA1 clusters is of the order of 10^2 torr and of the order of 10^{-20} torr for the associated dimer NA2DMA2.

As the saturation vapor pressure of AMP is lower than DMA, the clusters formed from AMP may have lower vapor pressure than those from DMA. Assuming that similar chemical mechanisms apply for AMP, we introduce NA1AMP1, with a saturation vapor pressure fixed at 9.75×10^{-8} torr and NA2AMP2 with a saturation vapor pressure fixed at 1.14×10^{-20} torr.

The formation of NA1AMP1 from the gas-phase reaction of HNO₃ with AMP is modelled following Carter (2008), as detailed in reaction (R1). A rate coefficient representative of radical + radical reactions is described in Carter (2008), with a value of $k_1 = 4.0 \times 10^{-11}$ cm³.molec⁻¹.s⁻¹, as an upper limit (Carter, 2008). The NA2AMP2 cluster is formed by combining two NA1AMP1 clusters, according to the reaction (R3). The addition of these new compounds is not limited to the formation of gaseous precursors according to kinetics. These compounds are then exposed to all associated physical processes described in the modules SCRAM, SOAP and H2O. Indeed, this implies that the compounds are all subject to a mechanistic representation of the physical processes governing aerosol evolution.

Respectively, we consider:

170 AMP +
$$HNO_3 \longrightarrow NA1AMP1$$
 (R1)



190

200

205



$$NA1AMP1 \longrightarrow AMP + HNO_3$$
 (R2)

$$NA1AMP1 + NA1AMP1 \longrightarrow NA2AMP2$$
 (R3)

$$175 \quad NA2AMP2 \longrightarrow NA1AMP1 + NA1AMP1 \tag{R4}$$

The kinetic coefficients presented for reactions R1 to R4 have been adapted to best represent the measurements and are presented in the results section in Table 7. Indeed, for reaction R1, the kinetic coefficient has been slightly decreased, remaining consistent with Carter (2008) arguments. The kinetic coefficients for reactions R2 and R4 are based on Chen et al. (2024) associated cluster evaporation rates. For the NA2AMP2 dimer, the value has been retained in view of the cluster's stability, unlike the case of NA1AMP1, where the constant has been slowed down to be more consistent with the characteristics of AMP compared with DMA and to enable a better fit with the experimental data. For the formation of the NA2AMP2 dimer (reaction R11), the kinetic coefficient was calibrated in order to fit the simulation to the experimental data included mass concentration of AMP, nitrate, organics, and particles total mass as well as mean diameter, total number of particles and granulometric repetition of particles number.

In order to accurately reproduce the evolution of the number of particles, a nucleation process is taken into account, with the parameterization chosen according to that defined in the model for organic compounds (Sartelet et al., 2025). This parameterization remains adjustable, with the power law exponent and scaling factor able to be defined. Particles formed by nucleation (small particles) are also subject to the Kelvin effect. In fact, a nucleation rate for the extremely-low volatility organic NA2AMP2 is added, and it is represented by a power law and a scaling factor. The power law is set as a squared power dependency:

$$J = K \times [\text{NA2AMP2}]^2 \tag{4}$$

where K represents the scaling factor. In the absence of an established mechanistic law, we propose choosing a quadratic dependence based on a bimolecular process hypothesis, which ensures realistic sensitivity of the nucleation rate with respect to concentrations. The values of K will be discussed in the results section and have been adjusted based on the experiments.

In the experiment of Tan et al. (2021), the ratio of AMP/nitrate averaged 1.6, indicating that the hypothesis of balanced clusters may not be the most appropriate here. The simulations carried out with the scheme described above lead to a significant difference in nitrate concentrations (see results section). However, quantum chemical calculations by Chen et al. (2018) and Chee et al. (2019) support that unbalanced clusters (like NA1DMA2 for example) can exist. These clusters may be more or less stable and probable. Indeed, in the case of DMA, the saturating vapour pressure associated with NA1DMA2 is of the order of 1×10^{-7} (torr), and therefore far too volatile to be considered here. Nevertheless, the different characteristics of AMP may suggest that a NA1AMP2 cluster could be more stable and much less volatile, and in this case be formed as well. The presence of a NA1AMP2 cluster would regulate the concentration of nitrates present in the particulate phase and equilibrate with NA1AMP1 and possibly NA2AMP2. We therefore propose to consider a NA1AMP1-type cluster in the modeling method, and to try to optimize the system as well as possible to determine if the method can re-equilibrate the nitrate mass. We therefore add the following to the chemical scheme included reactions R1 to R4:





$$NA1AMP1 + AMP \longrightarrow NA1AMP2$$
 (R5)

$$NA1AMP2 \longrightarrow NA1AMP1 + AMP \tag{R6}$$

For the NA1AMP2 cluster, the saturation vapor pressure was set at 6×10^{-16} (torr), using an approximation based on the equivalence of the 1:2 cluster to the saturation vapor pressure of the base aminium nitrate (1:1) between AMP and DMA. The lack of information on this type of cluster encouraged us to optimize the kinetic coefficients and nucleation rates according to the observation results. The calculation of the nucleation rate of NA1AMP2 follows the same method as that presented in equation (4). The best combinations of parameters, allowing representation of the peak on the number and an AMP/nitrate mass ratio consistent with the measurements, are presented in the results section in Table 7.

In order to take into account and test the two chemical mechanisms presented, the first one included reactions (R1) to (R4) and the second included (R1) to (R6), we propose to conduct two simulations, which we will designate simulation 1 and simulation 2.

2.3 Simulation setup

220 The simulation was set-up to reproduce the conditions of the chamber experiment of Tan et al. (2021).

2.3.1 Initial conditions

Gaseous initial conditions (presented in Table 2) have been extracted from PTR-MS-TOF mass spectrometer data at 07:48:00 for amine compounds, and from EUPHORE monitors for NO_x and O_3 Tan et al. (2021).

Table 2. Initial conditions for gaseous and particulate compounds extracted from measurement data at 2015-06-15 07:48:00 and from EUPHORE monitors for NO_x and O_3 . Concentrations are provided in $\mu g/m^3$ and calculated assuming $\rho = 1.0 \, g/cm^3$ for particulate initial conditions compounds following Tan et al. (2021).

Species	Concentration	Species	Concentration
NO_2	9.7	(CH ₃) ₂ (CHO)CNH ₂ (AMPal)	10.3
NO	12.1	(CH ₃) ₂ C=NH (P2IMI)	4.3
O_3	7.7	(CH ₃)(CH ₂ OH)C=NH (IPP)	0.8
AMP	449	(CH ₃) ₂ (CH ₂ OH)CNHNO ₂ (AMPNO2)	0.5
AMP (particle phase)	1.9	Nitrate (particle phase)	1.3

The modelled size distribution uses 80 size sections, logarithmically equally spaced from 1 nm to $2.5 \,\mu$ m (see appendix A).

The chemical speciation of the initial particles in the chamber was only aminium nitrates according to Tan et al. (2021). This latter is formed during the chamber preparation phase following the presumed injection of nitric acid accompanying NO as an





impurity. Figure 3 shows the distribution of number, surface and volume measured by the SMPS as a function of diameter at 07:47:00. This figure highlights the presence of a trimodal distribution, clearly visible by combining the three graphs. A part of the first peak is not visible here as it out of the measurement range of the instrument. It has been reconstructed using a classic log-normal law (eq. (5)), which was adjusted using nonlinear regression with the least-squares method and added to the initial conditions to be used in the simulation.

$$n(d) = \frac{N}{\sqrt{2\pi}\log(\sigma) \cdot d} \cdot \exp\left(-\frac{(\log(d/D_g))^2}{2(\log(\sigma))^2}\right)$$
 (5)

Figure 4 shows the mass and number distribution for initial particle conditions, including data inferred from the SMPS and the reconstruction of the first peak.

235 2.3.2 Meteorological data

The meteorological setup of the chamber is described in the supplementary materials of Tan et al. (2021). Values of temperature, pressure, relative and specific humidity are updated each $15 \, \text{min}$ during simulation. About photolysis rates, computed NO_2 photolysis rates at EUPHORE chamber location data have been compared to measured NO_2 photolysis rates from EUPHORE experiment. The ratio between the measured and computed NO_2 photolysis rates are lower than one, because of the cloud coverage. Hence this ratio was applied to correct all the photolysis rates in SSH-aerosol.

2.3.3 Hydroxyl radicals

240

245

Hydroxyl radicals (OH) levels are maintained constant by injection of Isopropyl nitrite ($CH_3CH(ONO)CH_3$, called IPN) during the whole experiment. Photolysis of IPN leads to the formation of acetone ($CH_3C(O)CH_3$), hydroperoxyl radical (HO_2) and nitrogen monoxide (NO), that react with each other to form OH (Raff and Finlayson-Pitts, 2010; Lannuque et al., 2021) as:

$$CH_3CH(ONO)CH_3 + h\nu \longrightarrow CH_3CH(O)CH_3 + NO$$
 (R7)

$$CH_3CH(O)CH_3 + O_2 \longrightarrow CH_3C(O)CH_3 + HO_2$$
 (R8)

$$250 \quad HO_2 + NO \longrightarrow OH + NO_2 \tag{R9}$$

During simulation, IPN photolysis is modeled by a continuous and direct emission of HO_2 , NO and acetone (decomposed as three PAR, following CB05 speciation matrix). This emission is set at $0.022 \,\mu\text{g/m}^3/\text{s}$ for HO_2 and NO and $0.065 \,\mu\text{g/m}^3/\text{s}$ for acetone, corresponding to an experimental injection of IPN of $0.3 \,\mu\text{L/min}$.

2.3.4 Representation and wall losses

In order to represent the concentrations in the chamber, auxiliary mechanism and wall losses of gas and particles are taken into account. For gaseous species, deposition processes are included via loss reactions implemented in the chemical scheme. From





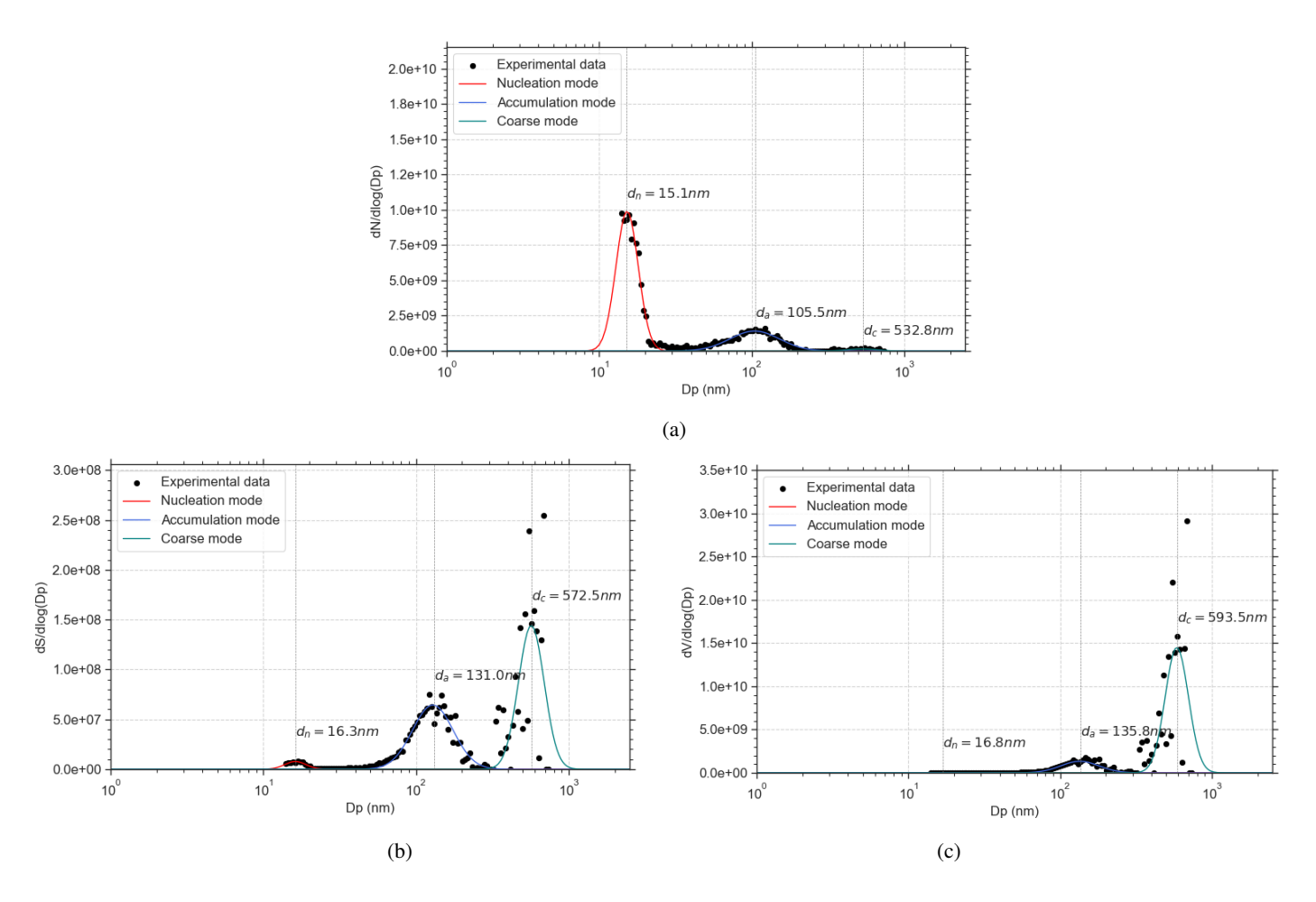


Figure 3. Representation of particle size distributions and modeled log-normal distributions for (a) number, (b) surface and (c) volume for initial conditions, in black dots the SMPS measurements, in red the nucleation mode, in blue the accumulation mode, in green the coarse mode

Bloss et al. (2005), the following specific mechanism has been added:

$$NO_2 \longrightarrow 0.5 \text{ HONO} + \text{wHNO}_3$$
 (R10)

260
$$O_3 \longrightarrow wO_3$$
 (R11)

$$HNO_3 \longrightarrow wHNO_3$$
 (R12)

$$AMP \longrightarrow wAMP$$
 (R13)

where species with a w in front represent the amount of material lost on the walls. The kinetic coefficients are taken from a characterization for EUPHORE (Bloss et al., 2005). For particles, a reference deposition velocity of $1 \times 10^{-5} \text{s}^{-1}$ is considered





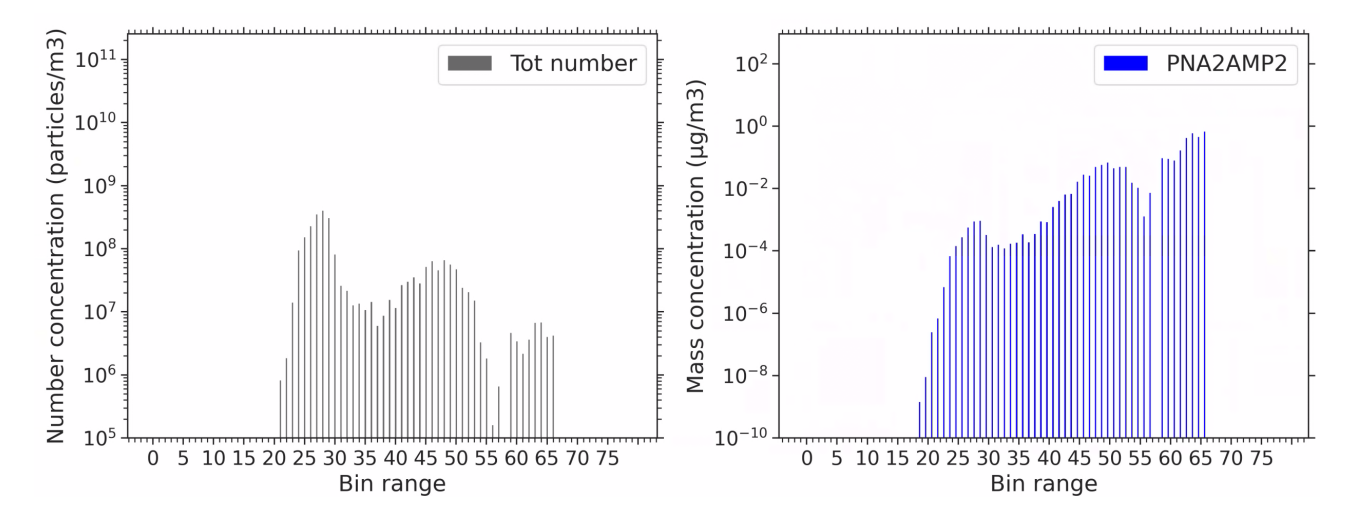


Figure 4. Initial conditions for number and mass concentration of aminium nitrate for each bin of the simulation.

for all particles and used through the SSH-model deposition module. This value is consistent with the average deposition velocities observed in the EUPHORE chamber (Wang et al., 2018). For AMP wall loss, Tan et al. (2021) estimate this value at $4-5\times10^{-5}~{\rm s}^{-1}$. This value was reduced because this constant was consuming an excessive amount of AMP.

Table 3. Kinetic rate constants in (in cm 3 .molecules $^{-1}$.s $^{-1}$ corresponding to wall losses, values adapted by equivalence with respect to volume/surface for particles loss rate in s $^{-1}$.

Reaction	Reference value	Adapted value
R10	1.5×10^{-5}	-
R11	3.8×10^{-6}	-
R12	8.2×10^{-5}	-
R13	4×10^{-5}	1.0×10^{-5}
Particle loss	1×10^{-5}	

270 3 Results and discussion

275

This section presents a comparison of the results obtained through simulation with SSH-aerosol to the measurements from the experiment conducted on June 15, 2015, at EUPHORE by Tan et al. (2021). In addition, simulation results are studied to assess the formation of carcinogenic compounds, as well as sensitivity to uncertainties and to the different processes considered. The following two statistical indicators will be used to evaluate the simulations: The relative bias on area under the curve "RBAUC" and NRMSE.





The relative bias on area under the curve (RBAUC) is defined as:

$$RBAUC = \left(\frac{AUC_{mod} - AUC_{obs}}{AUC_{obs}}\right) \times 100\%$$
(6)

where C_i^{mod} and C_i^{obs} be the modeled and observed concentrations respectively, measured at times t_i , for $i=0,1,\ldots,n$ and then AUC_{mod} and AUC_{obs} the associated area under the curve define using the trapezoidal rule as:

280 AUC
$$\approx \sum_{i=1}^{n} \frac{C_i + C_{i-1}}{2} \cdot (t_i - t_{i-1})$$
 (7)

The NRMSE is defined as the root mean square error normalized by the mean of the observed (experimental) values:

$$NRMSE = \frac{\sqrt{\frac{1}{n} \sum_{i=1}^{n} \left(C_i^{\text{mod}} - C_i^{\text{exp}} \right)^2}}{\frac{1}{n} \sum_{i=1}^{n} C_i^{\text{exp}}}$$
(8)

3.1 Ozone and nitrogen oxides

285

290

Firstly, an accurate representation of NO_x and O_3 , is necessary to reproduce the experimental conditions. The concentration profiles presented in Figure 5aa are all directly linked to the chemical mechanism implemented for AMP. O_3 is particularly dependent on this mechanism, as it is directly related to the level of volatile organic compounds (VOCs) available during the simulation. The VOCs levels are maintained primarily by the production of acetone resulting from the photolysis of IPN and secondarily by the VOCs formation during AMP gaseous degradation. Figure 5a shows the temporal evolution of the concentration profiles of ozone and nitrogen oxides for both simulated and measured data (a) and the simulated hydroxyl radicals profile (b).

Table 4. Statistical evaluation of simulated data for both simulations compared to measured data, BRAUC and NRMSE values for background species.

	Simul	ation 1	Simulation 2		
	BRAUC (%)	NRMSE (%)	BRAUC (%)	NRMSE (%)	
О3	18	20	16	19	
NO	-15	20	-14	19	
NO2	20	22	20	22	

The comparison of simulated and measured concentration profiles shows that the model is able to represent the general evolution of the three species, as presented in Table 4. NO_2 and O_3 are fairly well represented, with positive biases of the order of 20%. NO is slightly underestimated, as the lower values are less visible in Figure 5a. However, the assessment of these NO_2



310



and O_3 remains much the same between the two simulations. The average error is also in the same order of magnitude, around 20 %, which remains moderate and, in our case, relatively stable. The hydroxyl radicals simulated profile shows a variation of an order of magnitude between the beginning and the end of the simulation, indicating that the concentration level consistency is not maintained. An approximate representation of OH levels can have varying impacts on the rest of the chemistry, particularly on the degradation of AMP in this case. However, this profile cannot be evaluated due to the unavailability of measurements for this species during the experiment.

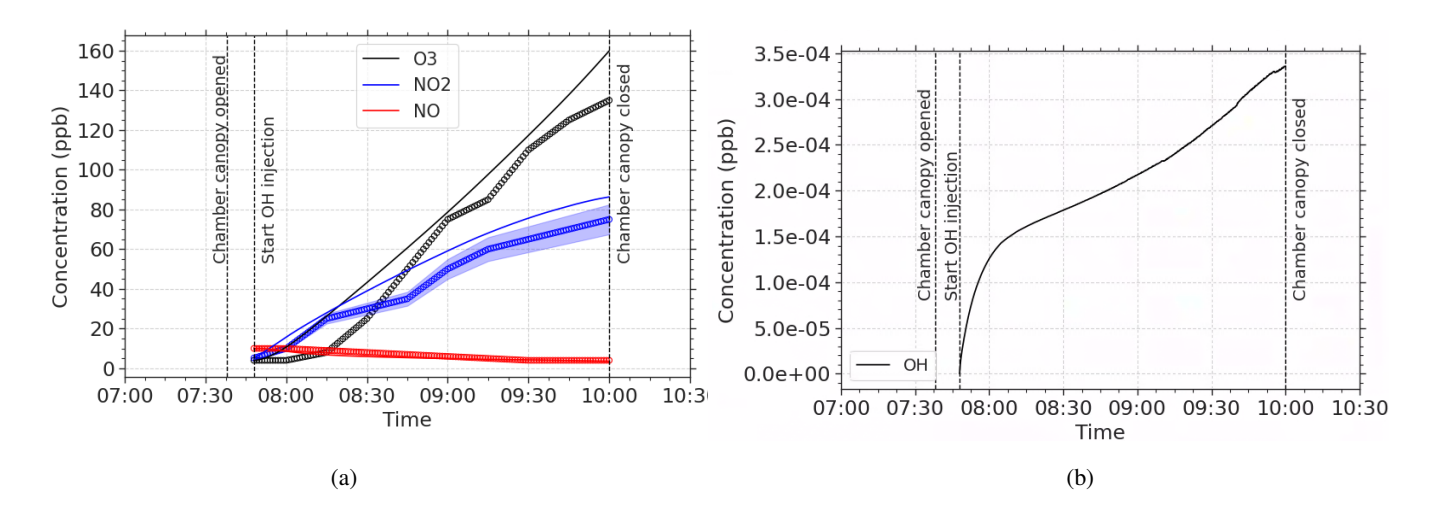


Figure 5. Measured (dotted curves) and simulated (solid line) temporal concentration profiles (in ppb) for ozone and nitrogen oxides (a). Observations are taken from Tan et al. (2021). Simulated temporal profiles for OH (b).

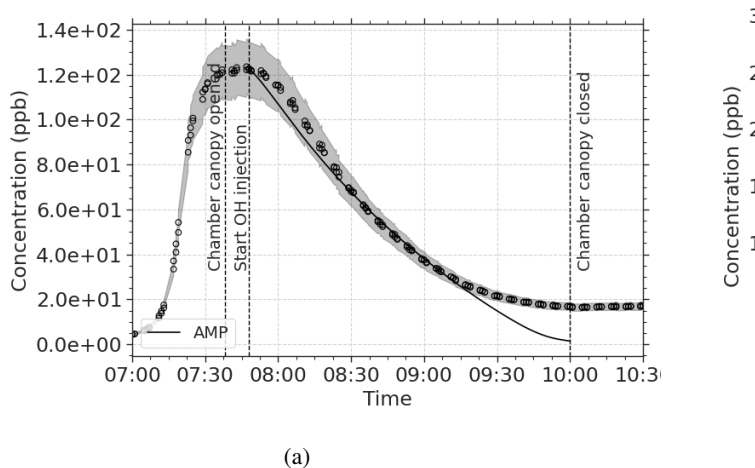
300 3.2 AMP and gaseous degradation products

Figure 6 shows the profile of AMP, which is well represented, with the largest model/measurement discrepancy at the end of the experiment after 9:30 hours. Concerning the end of the experiment, the concentrations are relatively low (5 times lower than at the 8 hours). This deviation could indicate that more AMP is degraded by oxidation with OH in the model than in the experiment, or that AMP measured concentrations could arise from elsewhere. Indeed, Tan et al. underline the very strong possibility of altering the AMP measurements by possible evaporation of the aminium salts in the sample line, thus leading to stabilization of the measured AMP concentration. Indeed, measurements performed with FTIR during the experiment show a continuous decrease in gaseous AMP, rather than a stabilization of concentrations as observed with PTR-MS measurements. As an optical instrument, FTIR is not affected by the possible evaporation of aminium salts in the sampling line, contrary to PTR-MS. This is confirmed by the low deviation observed for AMPal and P2IMI between simulation and measures.

The beginning of the simulation is characterized by a fast degradation of the AMP in the gas phase, slightly faster in the simulation than in the measurements as shown in figure 5a. The statistics, which are presented in Table 5 are very good for AMP, AMPal, P2IMI, but not for IPP, which is poorly represented in this mechanism. Furthermore, the results are fairly







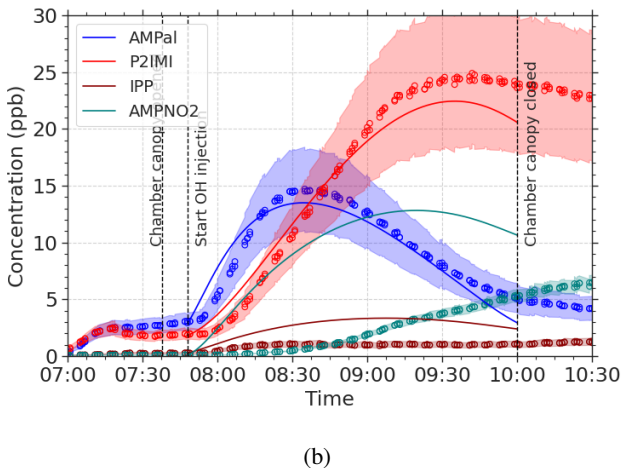


Figure 6. Measured (dotted curves) and simulated (solid lines) temporal concentration profiles (in ppb) for AMP (a) and for BCH3/BCH2/BNH2 = 6:70:24, AMPal (blue), P2IMI (red), IPP (dark red), and AMPNO2 (teal) (b). The shaded areas represent uncertainties of PTR-MS-TOF of 10% for calibrated species (AMP and AMPNO2) and 25% for others (Tan et al., 2021).

Table 5. Statistical evaluation of simulated data for both simulations compared to measured data, BRAUC and NRMSE values for gaseous AMP and degradation products.

	Simulation 1		Simulation 2			
	BRAUC (%)	NRMSE (%)	BRAUC (%)	NRMSE (%)		
AMP	-9	12	-10	12		
AMPal	-3	12	-5	13		
P2IMI	-3	10	-4	12		
IPP	186	198	181	193		

constant for both simulations. AMP, AMPal and P2IMI show very good performance, with less than 10% bias and around 10% relative error. Indeed, the major compounds, in this case AMPal and P2IMI, show a slight overestimation over the same period (5b). This discrepancy with measurements can be explained by the assumption of homogeneous mixing state in the simulation, whereas in the measurement, mixing is not instantaneous and perfectly homogeneous. However, the AMPal and P2IMI profiles remain well represented and are included in the measurement error bars contrary to IPP profile, where the simulation overestimates concentrations.

Another important aspect of Figure 6b is the representation of the concentration profiles of the nitramine associated with AMP (AMPNO2). Indeed, the comparison of these two profiles shows a significant discrepancy, up to 10 ppb above measurements around 9 a.m and 5 ppb above at the end of the experiment, indicating poor performance in the simulation of this species. However, Tan et al. (2021), through their modeling exercise of AMP oxidation with OH in the gas phase, present a



330



similar result for this species ith 8 ppb above measurements at around 9 a.m. and 3 ppb above at the end of the experiment, despite using a completely different model and chemistry modelling approach (MESMER). One explanation could be the difficulty of measuring nitramines, with a delayed instrumental response for this species in particular. Tan et al. (2021) report a response time of around 5 minutes for the experiment, and close to 1 hour for tests performed with AMPNO2 injected directly into the chamber, for both HT PTR-QMS and PTR-ToF-MS instruments. The last important species to be analysed is nitrosamines (AMPNO, (CH₃)₂(CH₂OH)CNHNO). However, there are no experimental data to prove the presence of this compound in the experiment. Tan et al. (2021) have not been able to measure AMPNO, potentially because it was below the instrument detection limit (about 50 ppt). Figure 7 shows the temporal profile of the modelled AMPNO concentration, which is very different from that of AMPNO2. A peak of 65 ppt is observed at the beginning of the experiment, then the concentration decreases rapidly to reach close to 0 ppt at the end of the experiment at 10:00:00 am. Reactions 8 and 9 from Table 1 explain the strong degradation of this molecule, particularly the photolysis process, in agreement with a short theoretical lifetime in the chamber close to 500s (Tan et al., 2021).

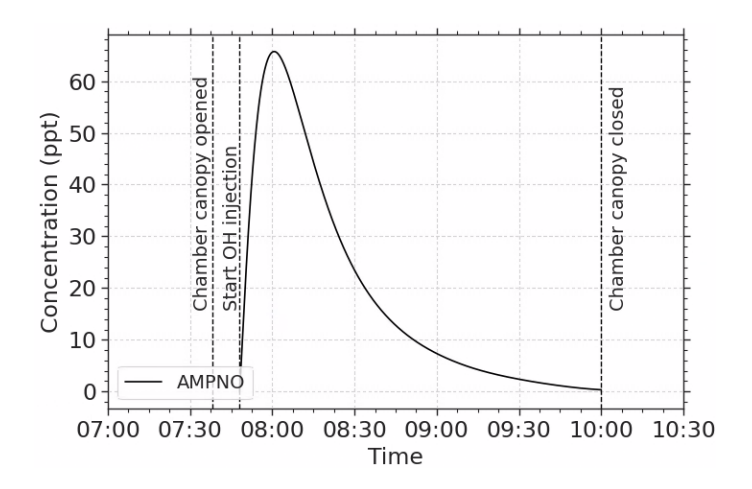


Figure 7. Simulated temporal concentration profile for nitrosamine (AMPNO, in ppt).

Table 6 shows the final concentrations for each compound followed during the simulation. In relation to the amount of AMP degraded by reaction with OH, at the end of the simulation, i.e. around 2h after the start, 138% of AMP was converted to nitramine for the both simulations and 0.002% for simulation 1 and 0.004% for simulation 2 to nitrosamine, these values taking into account the degradation of these compounds. These results are consistent, as the proportion of nitrosamine is very low due to its degradation by photolysis and OH, unlike nitramine, which is only degraded by reaction with OH. Atmospheric chamber conditions remain favorable to compounds degradations. Oxidant levels are higher and there is less competition between species than in free atmosphere. In addition, in the case of nitrosamines, their degradation is particularly pronounced during the day, as observed during this experiment.





Table 6. Concentrations of various compounds at the end of the simulation (10:00:00 am), concentrations in ppb.

Species Simulation 1		Simulation 2	Species	Simulation 1	Simulation 2	
AMP	1.50	4.44	AMPal	2.99	3.22	
P2IMI	20.93	20.56	IPP	2.43	2.43	
AMPNO2	10.83	10.78	AMPNO	1.6×10^{-3}	2.7×10^{-3}	

3.3 Secondary particles compounds

The strong formation of particles during this experiment, a phenomenon also observed in other projects (Nielsen et al., 2011; Murphy et al., 2007), can be a major degradation pathway for amines under atmospheric conditions. The values of the kinetic coefficients chosen for the two simulation methods are presented in the tables 7. Figure 8a shows the concentration profiles of AMP in particulate phase (PAMP) and Figure 8b nitrate (PNO3), total organic and total for all compounds, both for simulated data and measured data from the CHARON. In addition, the simulated concentration profiles presented take into account the specific CHARON size range.

Table 7. Kinetic rate constants in cm³.molecules⁻¹.s⁻¹ for bimolecular reactions and in s⁻¹ for unimolecular reactions, K_1 the scaling factor for NA2AMP2 nucleation, K_2 the scaling factor for NA1AMP2 nucleation.

Reaction	Simulation 1	Simulation 2
R9	0.8×10^{-12}	8.0×10^{-14}
R10	0.1×10^{1}	0.1×10^{1}
R11	1.9×10^{-14}	9.0×10^{-14}
R12	1.0×10^{-4}	1.0×10^{-4}
R13	_	1.5×10^{-14}
R14	_	1.0×10^{-3}
K_1	5.0×10^{-7}	1.0×10^{-7}
K_2	_	1.0×10^{-9}

The organic mass corresponds entirely to AMP in the case of our simulation, whereas during the experiment, the measured total organic concentration was higher than the measured AMP concentration, so other VOCs were present in non-negligible quantities (9% of the final mass). The lack of information on the VOCs present in the gaseous and particulate phases during the experiment, particularly at the beginning and consequently for the initial conditions in the simulation, makes it difficult to model and evaluate them. In fact, since total organics are relatively well reproduced, and inorganics are limited to nitrates in the case of simulation (because there is no formation of ammonium or other compounds), the deviation from measurement





for nitrates is transmitted to the total profile. The differences observed for nitrates are directly linked to the modelling choices made to represent aminium nitrates.

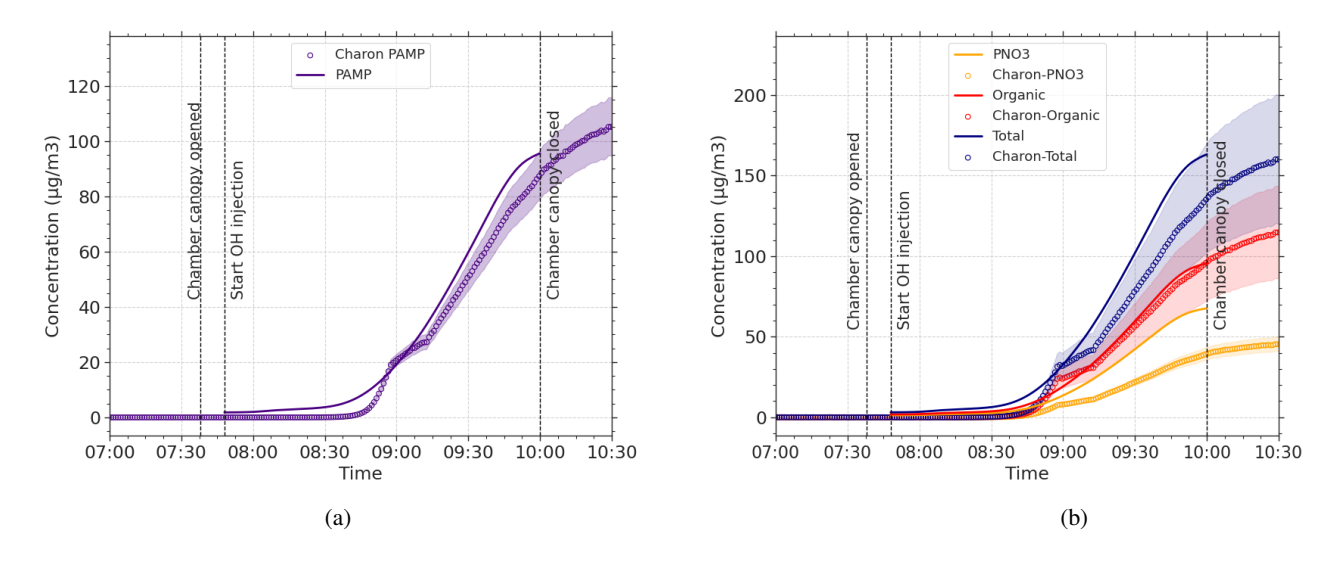


Figure 8. Measured (dotted curves) and simulated (solid lines) temporal concentration profiles for particulate AMP (violet)(in μ g/m³) (a) and for particulate nitrate (orange), total of organic compounds (red) and total particles (blue) (in μ g/m³) (b), corresponding to the reactions scheme presented in Table 7. The simulated concentrations are limited to the CHARON size range.

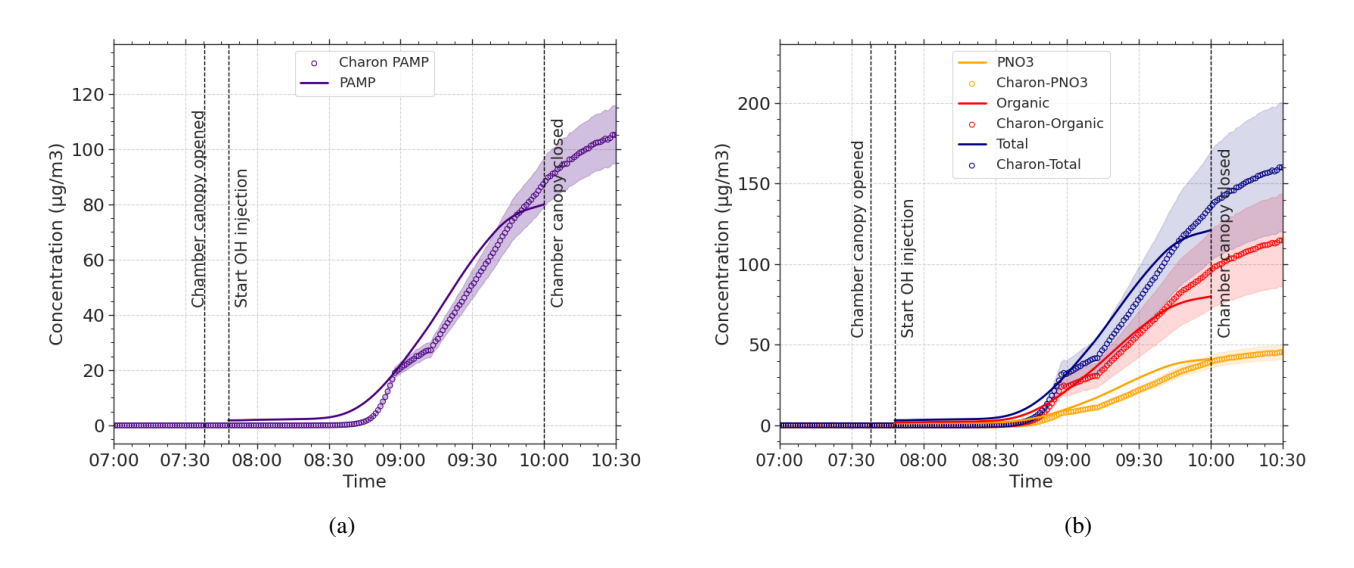


Figure 9. Measured (dotted curves) and simulated (solid lines) temporal concentration profiles for particulate AMP (violet)(in $\mu g/m^3$) (a) and for particulate nitrate (orange), total of organic compounds (red) and total particles (blue) (in $\mu g/m^3$) (b), for the simulation which include scheme presented in Table 7.



365

370



The graphs (a) and (b) in Figure 9 show the new mass concentration results simulated with the second reaction scheme. The general trends observed in these results have been reproduced. Indeed, the objective of simulation 2 seems to have been achieved, with nitrate and AMP concentrations both consistent with measurements, even if particle concentrations decrease at the end.

In Table 8, the final simulated concentrations are tabulated with the concentrations measured by the various instruments. The wrong representation of nitrates in simulation 1 has a strong impact on the aerosol total, while simulation 2 shows good results on nitrates, thus improving the score on the aerosol total. With regard to particulate AMP, the results are quite satisfactory in both simulations, with deviations ranging from 10% to 8%. Table 9 shows the statistical indicators over the experiment/simulation period for PAMP and PNO3, with simulation 2 improving the scores for both species. PAMP remains well represented, with less than 20% bias and error. The chemical mechanism chosen to better represent nitrates shows here a very good performance on PNO3 mass concentration, with a reduction in bias of almost 70% and relative error of over 100%. Furthermore, as previously mentioned, the probable evaporation of a fraction of the aminium salts in the sampling line implies an additional uncertainty that was not quantified during the experiment. However, the red curves in Figure (b) 8 and 9 of the organics in both simulations show that amines produce secondary VOCs, which can be derived from the various degradation products. However, modelling these compounds remains too complex for the time being, due to the lack of information on their nature and how they are formed.

Table 8. Concentrations of various compounds at 10:00:00 am from simulation and measurements with CHARON (in μg/m³).

Species SSH-aerosol		SH-aerosol SSH-aerosol CHARON Deviat		Deviation modelling/measure	Deviation modelling/measure	
	simulation 1	simulation 2		simulation 1	simulation 2	
Total PAMP	95.50	79.9	88.5	+8%	-10%	
Total PNO3	67.6	41.2	39.6	+70%	+4%	
Total Organic	95.5	78.9	97.1	-2%	-19%	
Total aerosol	163.1	121.1	136.7	+19%	-11%	

Table 9. Statistical evaluation of simulated data for both simulations compared to measured data, BRAUC and NRMSE values for particles mass, number and mean diameter.

	Simul	ation 1	Simulation 2		
	BRAUC (%) NRMSE (%)			NRMSE (%)	
PAMP	20	25	15	20	
PNO3	96	132	32	38	
Mean diameter	-10	15	-16	18	
Number total	Number total 8		46	55	



380

385

390



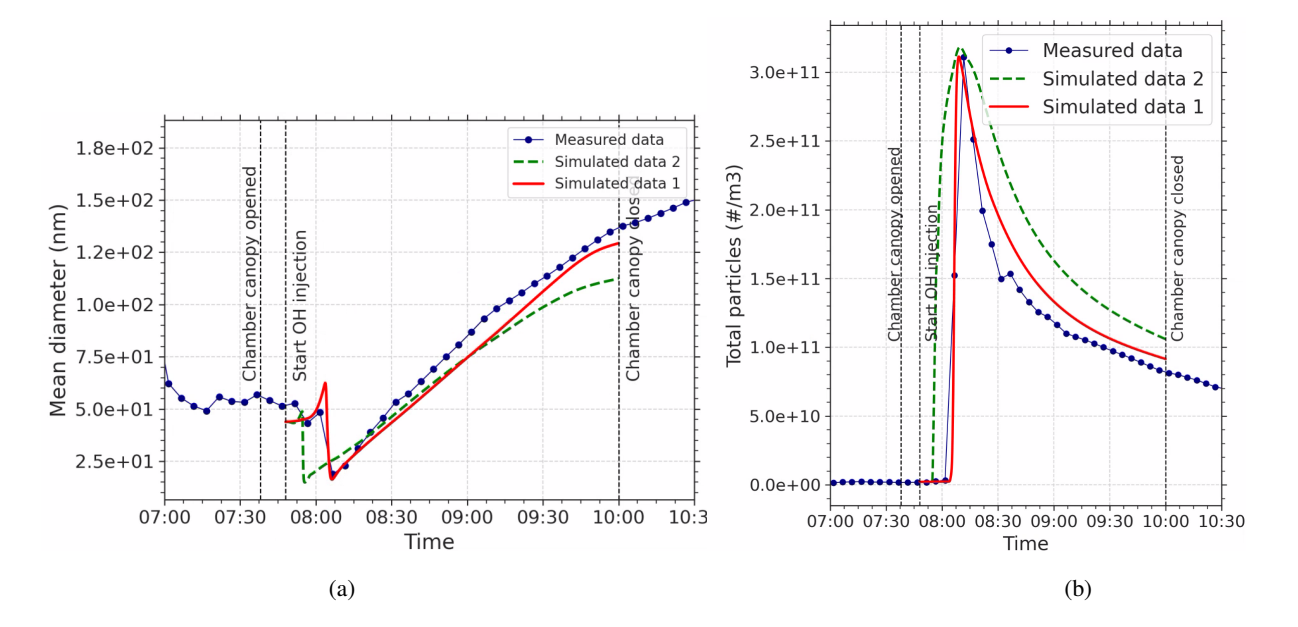


Figure 10. Measured (blue dotted curves) and simulated (red cross curves) temporal mean diameter profiles for SMPS size range (13 nm to 750 nm) (a) and temporal concentration profiles in terms of total number of particles (b).

Figure 10 shows the simulation results in red and green and the SMPS data in blue, (a) for the temporal evolution of the mean diameter and (b) for the temporal evolution of the total number of particles. In order to provide a fair comparison, the simulation data compared here only concern, as far as possible, bins coinciding with the measurement range of the instrument. In addition, for the simulated data, the average diameter was calculated by taking into account the number of particles associated with each bin (a bin representing a range of diameter sizes) and the average diameter of the bin in question, averaging the lower and upper bounds and is compared with the average diameters given by the SMPS. Figure 10 shows good results for model to measurement comparison for the mean diameter and the particle number concentrations for both simulations. Simulation 1 (with dimers only) shows very good results on both curves with more or less 10% on the bias, and respectively 15 and 35% error for diameter and number, apart from a slight discrepancy between 8:30 and 9:30, due to a too high number of small particles, which has a direct impact on the mean diameter. In simulation 2, the representation of the mean diameter and total number is less effective, with too many particles being formed too early compared with the measurements. However, the chosen configuration nonetheless enables the peak number to be represented, and thus maintains a consistent number of particles throughout the simulation. Simulation 2, as previously mentioned, is more complex to optimize. A right representation of the number confirms that the quantity of particles is consistent, and the diameter results confirm that the particles have an average particle size distribution that is also consistent with what was observed in the experiment. These curves were also decisive in the choice of the kinetic coefficients presented above. However, as can be seen from the statistical indicators in Table 9, the simulation performs less well on this point, particularly on the representation of the evolution of the total number, where the bias rises to 46% and the relative error to 55%, in agreement with what is observed on the green curves in Figure 10.





The particle size evolution remains fairly well represented, and the growth of particles observed via the increase in the mean diameter curve is in agreement with the measurements, as is the decrease in the number of particles over time. These two pieces of cross-referenced information imply that coagulation and nucleation plays a very important role here. Indeed, a simulation carried out without coagulation does not reproduce the decrease in number, and a simulation without nucleation is not able to represent the number evolution correctly, except by adding a consequent number of particles to the initial conditions, i.e. more than 10^{20} , which is not a coherent order of magnitude.

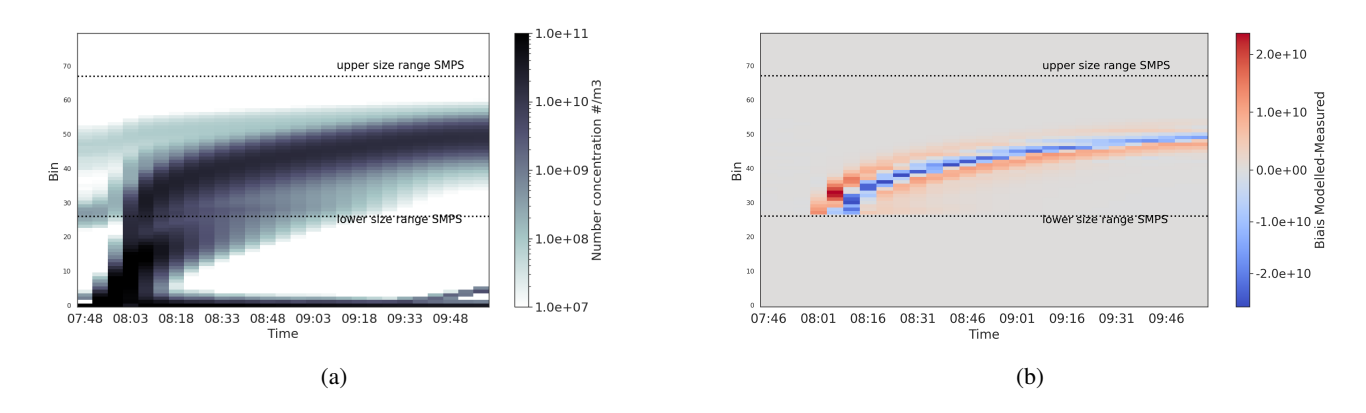


Figure 11. Modelled data and comparison to measurements: (a) particle number concentration and size distribution over time, and (b) bias relative to SMPS data, for simulation 1.

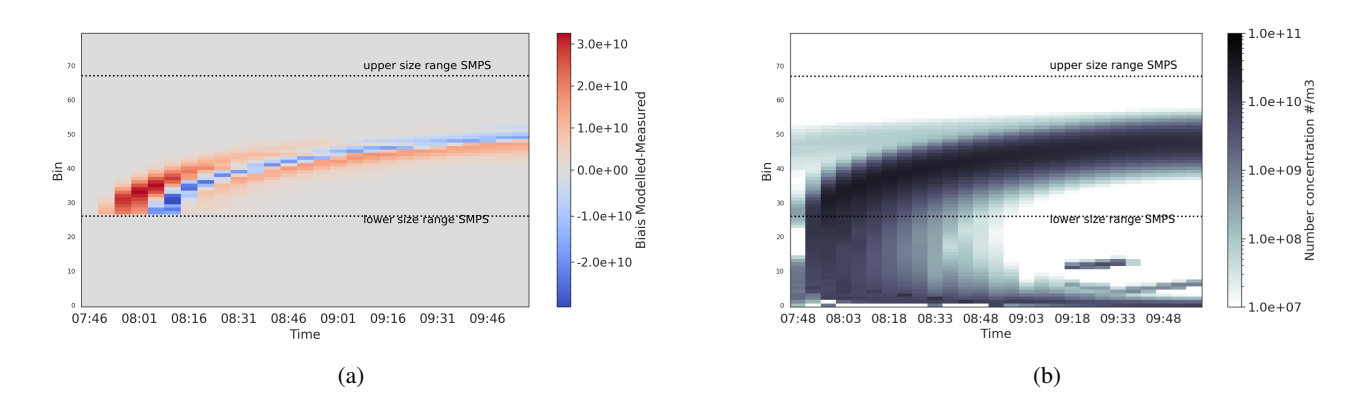


Figure 12. Modelled data and comparison to measurements: (a) particle number concentration and size distribution over time, and (b) bias relative to SMPS data, for simulation 2.

To complete the comparison in numbers, Figures 11 and 12 shows a representation of the temporal evolution of number concentrations by size bin as well as the bias with the measurements.



420



Bias representation (model-measurement) for the two simulations highlights that the number of particles is more concentrated over a smaller diameter range in the observation than in simulation, where the number concentrations are spread over a wider diameter range, still centred around the mean diameter.

However, the overall evolution of the experiment's particle population remains fairly well reproduced, with a fairly constant magnification over time. In addition, tests were carried out on the number of bins used, and the results between 40 and 80 bins remained similar. Increasing the granulometric discretization did not provide a better representation of particle distribution.

Table 10 shows the proportions of AMP degradation in particulate and gaseous phase for simulated and measured data. The proportions found for particulate degradation are in good agreement (less than 12% of error) with experimental estimates, as does the gaseous degradation of AMP, particularly for simulation 2.

Table 10. Percent of AMP transferred to the particles phase (AMP_{part}), undergoing gas phase reaction (AMP_{react}) and AMP wall loss (AMP_{wall}) for measured data at 10:11 am and simulated data at 10:00 am.

	AMP _{part}	AMPreact
Measured data	21	65
Simulated data 1	23	73
Simulated data 2	21	72

4 Conclusions

A multiphase chemistry of AMP has been developed and evaluated through the SSH-aerosol model by comparison with a controlled atmosphere experiment. Future deployment of amine scrubbing carbon capture processes will require knowledge to best assess the impacts of atmospheric emissions on people and the environment.

This study proposed a parametrisation for modelling the formation of particulate aminium nitrate in the gas and particle phases. In the context of a multiphasic model, 10 gas-phase species (AMP, AMPal, P2IMI, IPP, AMPN, AMPNO, AMPNO2) included aerosol precursor (NA1AMP1, NA2AMP2, NA1AMP2) involved in 18 different reactions (including nucleation) have been developed and implemented. The gaseous precursors can therefore be partitioned into the particulate phase (PNA1AMP1, PNA2AMP2, PNA1AMP2) according to the aerosol dynamics defined through the various SSH-aerosol modules.

The formation of molecular clusters NA_nAMP_m , where n and m correspond to the number of nitric acid and AMP molecules respectively, enabled consistent mass and number-based characterizations of aminium nitrate formation, while accounting for a dynamic partitioning between the gas and particulate phases. The formulations implemented for the mechanisms were based on molecular modeling results for a similar molecule, in the absence of specific data for AMP. The various kinetic coefficients and parameters of the power laws for nucleation were defined taking into account the most efficient simultaneous representation of the following concentration profiles: AMP gas phase and particulate phase, particulate phase nitrate, as well as the profiles



430

435



of the temporal evolution of the total number and average diameter. Simulation shows good performance in the temporal representation of particle number and size distribution. Using unbalanced clusters in the ageing process of AMP, leads to a good representation of the AMP/nitrate partitioning in the particulate phase.

Specifically with regard to nucleation, it would be important to conduct a series of experiments under different temperature conditions in order to adjust the power laws as accurately as possible. In addition, a quantum study specific to AMP would provide more reliable values for saturated vapor pressures and the stability of different clusters. Indeed, the parametrisations formulated in the context of indoor measurements are often complex to apply outdoors. (Sartelet et al., 2022)

In summary, although adjustments are needed to refine the modelling, the results obtained provide a solid basis for understanding the formation and degradation of secondary amine particles under atmospheric conditions and applying it in chemistry transport models. However, in the case of the atmosphere, amines can also undergo acid-base reactions with sulfuric acid. A similar method, certainly with a higher proportion of nucleation compared to what has been implemented for nitric acid, will have to be implemented.

In the context of future use of the model in a CTM coupling, comparison with measurements taken in the atmosphere, at ground level, and in plumes will be necessary to evaluate modeling methods or adjust them.





Appendix A: Simulation granulometric size range

Table A1. Granulometric correspondence of the bin bounds used in the simulation for a logarithmic distribution between 1nm and $2.5\mu m$. Diameter values are in nm, "LB" corresponds to the lower bound and "UB" to the upper bound.

Bin	LB	UB	Bin	LB	UB	Bin	LB	UB	Bin	LB	UB
0	1.00	1.10	25	11.53	12.72	50	132.96	146.62	75	1533.09	1690.61
1	1.10	1.22	26	12.72	14.02	51	146.62	161.68	76	1690.61	1864.31
2	1.22	1.34	27	14.02	15.46	52	161.68	178.29	77	1864.31	2055.85
3	1.34	1.48	28	15.46	17.05	53	178.29	196.61	78	2055.85	2267.07
4	1.48	1.63	29	17.05	18.80	54	196.61	216.81	79	2267.07	2500.00
5	1.63	1.80	30	18.80	20.73	55	216.81	239.09			
6	1.80	1.98	31	20.73	22.87	56	239.09	263.65			
7	1.98	2.19	32	22.87	25.21	57	263.65	290.74			
8	2.19	2.41	33	25.21	27.81	58	290.74	320.61			
9	2.41	2.66	34	27.81	30.66	59	320.61	353.55			
10	2.66	2.93	35	30.66	33.81	60	353.55	389.88			
11	2.93	3.23	36	33.81	37.29	61	389.88	429.94			
12	3.23	3.57	37	37.29	41.12	62	429.94	474.11			
13	3.57	3.93	38	41.12	45.34	63	474.11	522.82			
14	3.93	4.34	39	45.34	50.00	64	522.82	576.54			
15	4.34	4.78	40	50.00	55.14	65	576.54	635.77			
16	4.78	5.27	41	55.14	60.80	66	635.77	701.09			
17	5.27	5.81	42	60.80	67.05	67	701.09	773.12			
18	5.81	6.41	43	67.05	73.94	68	773.12	852.56			
19	6.41	7.07	44	73.94	81.53	69	852.56	940.15			
20	7.07	7.80	45	81.53	89.91	70	940.15	1036.74			
21	7.80	8.60	46	89.91	99.15	71	1036.74	1143.26			
22	8.60	9.48	47	99.15	109.34	72	1143.26	1260.72			
23	9.48	10.46	48	109.34	120.57	73	1260.72	1390.26			
24	10.46	11.53	49	120.57	132.96	74	1390.26	1533.09			

Author contributions. DL, YR, and OD designed the research topic; DL, KS, and YR worked on developing the model and reaction schemes.;

440 DL performed the simulations and analyze data with KS and YR; DL, YR and KS wrote the manuscript draft.





Competing interests. The authors declare that they have no conflict of interest.

Acknowledgements. We would like to thank Armin Wisthaler and Claus Jørgen Nielsen for providing us with detailed data from their experiment; Donny Cooper and John Snyder from Houston research center US-TEPTR (TotalEnergies Production and Refining in the United States) for supporting the technical aspects of installing models on their HPC environment, where we performed the simulations; Youngseob Kim and Florian Couvidat for providing information on the structure of the model; TotalEnergies for its financial support.





References

- Alam, A.: Monitoring a New Benchmark Solvent for CO2 Capture: Pushing Technical Boundaries, Master's thesis, University of South-Eastern Norway, 2024.
- Backes, A. M., Aulinger, A., Bieser, J., Matthias, V., and Quante, M.: Ammonia emissions in Europe, part II: How ammonia emission abatement strategies affect secondary aerosols, Atmospheric Environment, 126, 153–161, 2016.
 - Benquet, C., Knarvik, A. B. N., Gjernes, E., Hvidsten, O. A., Romslo Kleppe, E., and Akhter, S.: First process results and operational experience with CESAR1 solvent at TCM with high capture rates (ALIGN-CCUS project), in: Proceedings of the 15th Greenhouse Gas Control Technologies Conference, pp. 15–18, 2021.
- Bloss, C., Wagner, V., Bonzanini, A., Jenkin, M., Wirtz, K., Martin-Reviejo, M., and Pilling, M.: Evaluation of detailed aromatic mechanisms (MCMv3 and MCMv3. 1) against environmental chamber data, Atmospheric Chemistry and Physics, 5, 623–639, 2005.
 - Bouckaert, Pales, F., McGlade, Remme, and Wanner: Net Zero by 2050: A Roadmap for the Global Energy Sector, IEA, 2021.
 - Brúder, P., Grimstvedt, A., Mejdell, T., da Silva, E. F., and Svendsen, H. F.: CO2 capture into aqueous solutions of the mixed solvent Cesar 1, in: Proceedings of the 2nd Annual Gas Processing Symposium, pp. 31–40, Elsevier, 2010.
- 460 Carter, W. P.: Reactivity estimates for selected consumer product compounds, Final Report to the California Air Resources Board Contract, 2008.
 - Chamba, G., Rissanen, M., Barthelmeß, T., Saiz-Lopez, A., Rose, C., Iyer, S., Saint-Macary, A., Rocco, M., Safi, K., Deppeler, S., Barr, N., Harvey, M., Engel, A., Dunne, E., Law, C., and Sellegri, K.: Evidence of nitrate-based nighttime atmospheric nucleation driven by marine microorganisms in the South Pacific, Proc Natl Acad Sci U S A., 120, e2308696 120, https://doi.org/10.1073/pnas.2308696120, 2023.
- Chee, S., Myllys, N., Barsanti, K. C., Wong, B. M., and Smith, J. N.: An experimental and modeling study of nanoparticle formation and growth from dimethylamine and nitric acid, The Journal of Physical Chemistry A, 123, 5640–5648, 2019.
 - Chen, D.-P., Ma, W., Yang, C.-H., Li, M., Zhou, Z.-Z., Zhang, Y., Wang, X.-C., and Quan, Z.-J.: Formation of atmospheric molecular clusters containing nitric acid with ammonia, methylamine, and dimethylamine, Environmental Science: Processes & Impacts, 26, 2036–2050, 2024.
- 470 Chen, K., Zhang, K., and Qiu, C.: Potential enhancement in atmospheric new particle formation by amine-assisted nitric acid condensation at room temperature, Atmospheric Environment, 287, 119 252, https://doi.org/https://doi.org/10.1016/j.atmosenv.2022.119252, 2022.
 - Chen, X., Huang, G., An, C., Yao, Y., and Zhao, S.: Emerging N-nitrosamines and N-nitramines from amine-based post-combustion CO2 capture–a review, Chemical Engineering Journal, 335, 921–935, 2018.
- Couvidat, F. and Sartelet, K.: The Secondary Organic Aerosol Processor (SOAP v1. 0) model: a unified model with different ranges of complexity based on the molecular surrogate approach, Geoscientific Model Development, 8, 1111–1138, 2015.
 - Couvidat, F., Debry, E., Sartelet, K., and Seigneur, C.: A hydrophilic/hydrophobic organic (H2O) aerosol model: Development, evaluation and sensitivity analysis, Journal of Geophysical Research: Atmospheres, 117, 2012.
 - Drewnick, F., Hings, S. S., DeCarlo, P., Jayne, J. T., Gonin, M., Fuhrer, K., Weimer, S., Jimenez, J. L., Demerjian, K. L., Borrmann, S., et al.: A new time-of-flight aerosol mass spectrometer (TOF-AMS)—Instrument description and first field deployment, Aerosol Science and Technology, 39, 637–658, 2005.
 - Eichler, P., Müller, M., D'anna, B., and Wisthaler, A.: A novel inlet system for online chemical analysis of semi-volatile submicron particulate matter, Atmospheric Measurement Techniques, 8, 1353–1360, 2015.





- Erisman, J. and Schaap, M.: The need for ammonia abatement with respect to secondary PM reductions in Europe, Environmental Pollution, 129, 159–163, 2004.
- Fredriksen, S. and Jens, K.-J.: Oxidative degradation of aqueous amine solutions of MEA, AMP, MDEA, Pz: A review, Energy Procedia, 37, 1770–1777, 2013.
 - Ge, X., Wexler, A. S., and Clegg, S. L.: Atmospheric amines Part II. Thermodynamic properties and gas/particle partitioning, Atmospheric Environment, 45, 561–577, https://doi.org/https://doi.org/10.1016/j.atmosenv.2010.10.013, 2011.
- Gjernes, E., Helgesen, L. I., and Maree, Y.: Health and environmental impact of amine based post combustion CO2 capture, Energy Procedia, 37, 735–742, 2013.
 - Gouedard, C., Picq, D., Launay, F., and Carrette, P.-L.: Amine degradation in CO2 capture. I. A review, International journal of greenhouse gas control, 10, 244–270, 2012.
 - Heo, J., McCoy, S. T., and Adams, P. J.: Implications of ammonia emissions from post-combustion carbon capture for airborne particulate matter, Environmental science & technology, 49, 5142–5150, 2015.
- 495 Karl, M., Wright, R. F., Berglen, T. F., and Denby, B.: Worst case scenario study to assess the environmental impact of amine emissions from a CO2 capture plant, International Journal of Greenhouse Gas Control, 5, 439–447, 2011.
 - Karl, M., Dye, C., Schmidbauer, N., Wisthaler, A., Mikoviny, T., d'Anna, B., Müller, M., Borrás, E., Clemente, E., Muñoz, A., et al.: Study of OH-initiated degradation of 2-aminoethanol, Atmospheric chemistry and physics, 12, 1881–1901, 2012.
 - Karl, M., Castell, N., Simpson, D., Solberg, S., Starrfelt, J., Svendby, T., Walker, S.-E., and Wright, R. F.: Uncertainties in assessing the environmental impact of amine emissions from a CO₂ capture plant, Atmospheric Chemistry and Physics, 14, 8533–8557, 2014.
 - Karl, M., Svendby, T., Walker, S.-E., Von Streng Velken, A., Castell, N., and Solberg, S.: Modelling atmospheric oxidation of 2-aminoethanol (MEA) emitted from post-combustion capture using WRF–Chem, Science of the Total Environment, 527, 185–202, 2015.
 - Knudsen, S., Cassiani, M., Karl, M., Slørdal, L. H., and Tarrasón, L.: CO2 Capture Mongstad Project/HETQPAmine2. Modelling atmospheric dispersion for components from post combustion amine based CO2 capture., NILU OR, 2010.
- Koiwanit, J., Supap, T., Chan, C., Gelowitz, D., Idem, R., and Tontiwachwuthikul, P.: An expert system for monitoring and diagnosis of ammonia emissions from the post-combustion carbon dioxide capture process system, International Journal of Greenhouse Gas Control, 26, 158–168, 2014.
 - Kumar, M., Li, H., Zhang, X., Zeng, X. C., and Francisco, J. S.: Nitric acid–amine chemistry in the gas phase and at the air–water interface, Journal of the American Chemical Society, 140, 6456–6466, 2018.
- Lannuque, V. and Sartelet, K.: Development of a detailed gaseous oxidation scheme of naphthalene for secondary organic aerosol (SOA) formation and speciation, 24, 8589–8606, https://doi.org/10.5194/acp-24-8589-2024, 2024.
 - Lannuque, V., D'anna, B., Couvidat, F., Valorso, R., and Sartelet, K.: Improvement in modeling of oh and ho2 radical concentrations during toluene and xylene oxidation with racm2 using mcm/gecko-a, Atmosphere, 12, 732, 2021.
- Lannuque, V., D'Anna, B., Kostenidou, E., Couvidat, F., Martinez-Valiente, A., Eichler, P., Wisthaler, A., Müller, M., Temime-Roussel, B., Valorso, R., and Sartelet, K.: Gas-particle partitioning of toluene oxidation products: an experimental and modeling study, 23, 15 537–15 560, https://doi.org/10.5194/acp-23-15537-2023, 2023.
 - Li, K., White, S., Zhao, B., Geng, C., Halliburton, B., Wang, Z., Zhao, Y., Yu, H., Yang, W., Bai, Z., et al.: Evaluation of a new chemical mechanism for 2-amino-2-methyl-1-propanol in a reactive environment from CSIRO smog chamber experiments, Environmental Science & Technology, 54, 9844–9853, 2020.



530

535

550



- Manzolini, G., Fernandez, E. S., Rezvani, S., Macchi, E., Goetheer, E., and Vlugt, T.: Economic assessment of novel amine based CO2 capture technologies integrated in power plants based on European Benchmarking Task Force methodology, Applied Energy, 138, 546–558, 2015.
 - Manzoor, S., Korre, A., Durucan, S., and Simperler, A.: Atmospheric chemistry modelling of amine emissions from post combustion CO2 capture technology, Energy Procedia, 63, 822–829, 2014.
- Martin, S., Lepaumier, H., Picq, D., Kittel, J., de Bruin, T., Faraj, A., and Carrette, P.-L.: New amines for CO2 capture. IV. Degradation, corrosion, and quantitative structure property relationship model, Industrial & engineering chemistry research, 51, 6283–6289, 2012.
 - Metz, B., Davidson, O., de Coninck, H., Loos, M., and Meyer, L.: IPCC Special Report on Carbon Dioxide Capture and Storage. Prepared by Working Group III of the Intergovernmental Panel on Climate Change, Cambridge University Press, 2005.
 - Murphy, S., Sorooshian, A., Kroll, J., Ng, N., Chhabra, P., Tong, C., Surratt, J., Knipping, E., Flagan, R., and Seinfeld, J.: Secondary aerosol formation from atmospheric reactions of aliphatic amines, Atmospheric Chemistry and Physics, 7, 2313–2337, 2007.
 - Nenes, A., Pandis, S. N., and Pilinis, C.: ISORROPIA: A new thermodynamic equilibrium model for multiphase multicomponent inorganic aerosols, Aquatic geochemistry, 4, 123–152, 1998.
 - Nielsen, C., D'Anna, B., Bossi, R., Bunkan, A., Dithmer, L., Glasius, M., Hallquist, M., Hansen, A., Lutz, A., Salo, K., et al.: Atmospheric Degradation of Amines (ADA) Summary report from atmospheric chemistry studies of amines, nitrosamines, nitramines and amides, CLIMIT project no. 208122, CLIMIT project, 2011.
 - Nielsen, C. J., D'Anna, B., Dye, C., George, C., Graus, M., Hansel, A., Karl, M., King, S., Musabile, M., Muller, M., et al.: Atmospheric Degradation of Amines (ADA). Summary report: Gas phase photo-oxidation of 2-aminoethanol (MEA) CLIMIT project no. 193438., NILU OR, 2010.
 - Qiu, C. and Zhang, R.: Multiphase chemistry of atmospheric amines, Physical Chemistry Chemical Physics, 15, 5738–5752, 2013.
- Raff, J. D. and Finlayson-Pitts, B. J.: Hydroxyl radical quantum yields from isopropyl nitrite photolysis in air, Environmental science & technology, 44, 8150–8155, 2010.
 - Rao, A. B. and Rubin, E. S.: A technical, economic, and environmental assessment of amine-based CO2 capture technology for power plant greenhouse gas control, Environmental science & technology, 36, 4467–4475, 2002.
 - Rochelle, G. T.: Thermal degradation of amines for CO2 capture, Current Opinion in Chemical Engineering, 1, 183-190, 2012.
- Sartelet, K., Couvidat, F., Wang, Z., Flageul, C., and Kim, Y.: SSH-aerosol v1. 1: A modular box model to simulate the evolution of primary and secondary aerosols, Atmosphere, 11, 525, 2020.
 - Sartelet, K., Kim, Y., Couvidat, F., Merkel, M., Petäjä, T., Sciare, J., and Wiedensohler, A.: Influence of emission size distribution and nucleation on number concentrations over Greater Paris, Atmospheric Chemistry and Physics Discussions, 2022, 1–24, 2022.
 - Sartelet, K., Wang, Z., Lannuque, V., Iyer, S., Couvidat, F., and Sarica, T.: Modelling molecular composition of SOA from toluene photo-oxidation at urban and street scales, Environ. Sci.: Atmos., 4, 839–847, https://doi.org/10.1039/D4EA00049H, 2024.
 - Sartelet, K., Wang, Z., Kim, Y., Lannuque, V., and Couvidat, F.: Advanced modeling of gas chemistry and aerosol dynamics with SSH-aerosol v2.0, EGUsphere, 2025, 1–41, https://doi.org/10.5194/egusphere-2025-2191, 2025.
 - Sharma, S. D. and Azzi, M.: A critical review of existing strategies for emission control in the monoethanolamine-based carbon capture process and some recommendations for improved strategies, Fuel, 121, 178–188, https://doi.org/https://doi.org/10.1016/j.fuel.2013.12.023, 2014.
 - Shen, X., Chen, J., Li, G., and An, T.: A new advance in the pollution profile, transformation process, and contribution to aerosol formation and aging of atmospheric amines, Environmental Science: Atmospheres, 3, 444–473, 2023.





- Strazisar, B. R., Anderson, R. R., and White, C. M.: Degradation pathways for monoethanolamine in a CO2 capture facility, Energy & fuels, 17, 1034–1039, 2003.
- Tan, W., Zhu, L., Mikoviny, T., Nielsen, C. J., Wisthaler, A., D'anna, B., Antonsen, S., Stenstrøm, Y., Farren, N. J., Hamilton, J. F., et al.: Experimental and theoretical study of the OH-initiated degradation of piperazine under simulated atmospheric conditions, The Journal of Physical Chemistry A, 125, 411–422, 2020.
 - Tan, W., Zhu, L., Mikoviny, T., Nielsen, C. J., Tang, Y., Wisthaler, A., Eichler, P., Muller, M., D'anna, B., Farren, N. J., et al.: Atmospheric chemistry of 2-amino-2-methyl-1-propanol: a theoretical and experimental study of the OH-initiated degradation under simulated atmospheric conditions, The Journal of Physical Chemistry A, 125, 7502–7519, 2021.
 - Thong, D., Dave, N., Feron, P., and Azzi, M.: Environmental Impacts of Amine-Based CO2 Post Combustion Capture (PCC) Process, Report to ANLECR&D, 2012.
 - Vevelstad, S. J., Eide-Haugmo, I., da Silva, E. F., and Svendsen, H. F.: Degradation of MEA; a theoretical study, Energy Procedia, 4, 1608–1615, 2011.
- Wang, N., Jorga, S. D., Pierce, J. R., Donahue, N. M., and Pandis, S. N.: Particle wall-loss correction methods in smog chamber experiments, Atmospheric Measurement Techniques, 11, 6577–6588, 2018.
 - Wang, Z., Couvidat, F., and Sartelet, K.: Implementation of a parallel reduction algorithm in the GENerator of reduced Organic Aerosol mechanisms (GENOA v2.0): Application to multiple monoterpene aerosol precursors, 174, 106248, https://doi.org/10.1016/j.jaerosci.2023.106248, 2023.
- Yarwood, G., Rao, S., Yocke, M., and Whitten, G.: Updates to the carbon bond chemical mechanism: CB05, Final report to the US EPA, RT-0400675, 8, 13, 2005.
 - Yu, K., Mitch, W. A., and Dai, N.: Nitrosamines and nitramines in amine-based carbon dioxide capture systems: fundamentals, engineering implications, and knowledge gaps, Environmental Science & Technology, 51, 11522–11536, 2017.
- Zhu, S., Sartelet, K., and Seigneur, C.: A size-composition resolved aerosol model for simulating the dynamics of externally mixed particles: SCRAM (v 1.0), Geosci. Model Dev., 8, 1595–1612, 2015.